

# NJC

Accepted Manuscript



This is an *Accepted Manuscript*, which has been through the Royal Society of Chemistry peer review process and has been accepted for publication.

*Accepted Manuscripts* are published online shortly after acceptance, before technical editing, formatting and proof reading. Using this free service, authors can make their results available to the community, in citable form, before we publish the edited article. We will replace this *Accepted Manuscript* with the edited and formatted *Advance Article* as soon as it is available.

You can find more information about *Accepted Manuscripts* in the [Information for Authors](#).

Please note that technical editing may introduce minor changes to the text and/or graphics, which may alter content. The journal's standard [Terms & Conditions](#) and the [Ethical guidelines](#) still apply. In no event shall the Royal Society of Chemistry be held responsible for any errors or omissions in this *Accepted Manuscript* or any consequences arising from the use of any information it contains.



Journal Name

ARTICLE

## Sustainable Starch Modified Polyol Based Tough Biocompatible Hyperbranched Polyurethane with Shape Memory Attribute

Rituparna Duarah,<sup>a</sup> Yogendra Pratap Singh,<sup>b</sup> Biman B. Mandal<sup>b</sup> and Niranjana Karak<sup>a\*</sup>Received 00th January 20xx,  
Accepted 00th January 20xx

DOI: 10.1039/x0xx00000x

www.rsc.org/

In the recent years, the application of shape memory polymers (SMPs) gained substantial impetus for design of improved and minimally invasive smart biomedical implant devices based on their thermal response behavior. In this direction, the authors designed a tough, biodegradable and biocompatible shape memory hyperbranched polyurethane (HPU) suitable for use in medical implant devices. HPUs with three different compositions containing 11, 14 and 17 wt.% of starch modified polyol as the branch generating moiety were synthesized *via* A<sub>x</sub> + B<sub>y</sub> (x, y ≥ 2) approach, without the use of any plasticizer or catalyst. The structures of the synthesized HPU were confirmed from FTIR, NMR and various analytical studies. The biodegradable HPU exhibited combined attributes of remarkable mechanical properties (17 MPa tensile strength, 1450% elongation at break, 6.5 kg scratch hardness, >100 cm impact strength and 163 MJ m<sup>-3</sup> toughness) at room temperature and desired shape memory behavior (98.8% shape fixity and 98.9% shape recovery) at around body temperature (37 ± 1) °C. No significant change in mechanical performance was also observed under wet condition. Moreover, cell proliferation and live/dead cell viability assays confirmed biocompatibility of the synthesized HPU. Thus, the overall results indicated its potential application as an advanced material in the field of biomedical.

### Introduction

Shape memory polymer (SMP) is a unique class of highly functional smart materials capable of changing a predetermined temporary shape to its original permanent shape on exposure to a suitable external stimulus like heat,<sup>1</sup> light,<sup>2</sup> microwave<sup>3</sup> etc. Over the last decade, thermally induced SMPs gained substantial impetus for designing next generation minimally invasive smart medical implants, in the field of biomedical applications.<sup>4</sup> However, the increase in depletion of petroleum resources and threat of global warming compelled the society to prioritize the use of renewable resources for development of bio-based SMPs using novel and innovative technologies.<sup>1</sup>

In the current scenario, specially designed bio-based thermally induced shape memory hyperbranched polyurethane (HPU) emerged as a potential candidate owing to its sharp transition temperature of shape recovery, excellent recoverable strain (up to 400%), high control of retraction and softening temperatures, inherent soft-hard segments, low viscosity and high solubility.<sup>1,5,6</sup> Thus, in this investigation, a simple strategy was reported to obtain a SMP by synthesizing a starch modified polyol based HPU with

remarkable mechanical properties, biocompatibility, biodegradability and almost complete shape recovery. Being a promising, abundant, eco-friendly, and economically viable natural renewable resource, the use of starch in hyperbranched polyol is advantageous as it may impart biodegradability and biocompatibility to the final product.<sup>7,8</sup> In 2008, Wu et al. cross-linked thermoplastic-polyurethane micro particles with the starch matrix through urethane linkages to improve the toughness of the resultant thermoplastic.<sup>9</sup> In 2009, Da Roz et al. obtained cross-linked starch/polyurethane plastics by the direct polymerization of corn starch and oligomeric diisocyanate with slightly improved elastomeric property.<sup>10</sup> Thus when starch was used as a major component to modify polyurethane, the resultant products displayed overall poor performance along with processing difficulties owing to the brittleness, hydrophilicity, plasticization and solubility problem in various organic solvents of starch.<sup>11</sup> Moreover, no report on starch modified polyurethanes with unique hyperbranched architecture and shape memory attributes, was found. Thus, in the present study, starch was used as a reactant in a hydrolyzed hyperbranched epoxy to obtain the desired hyperbranched polyol. This hyperbranched polyol was subsequently used for synthesizing HPU, without the use of any plasticizer or catalyst. In this milieu, the use of various bio-based raw materials including vegetable oil was reported for the synthesis of shape memory HPUs.<sup>12</sup> In 2014, Kalita et al. used monoglycerides of various vegetable oils for synthesizing different HPUs which exhibited high tensile strength and good shape recovery and shape fixity at 60 °C.<sup>13</sup> However, such bio-based thermally induced SMPs did not

<sup>a</sup>Advanced Polymer and Nanomaterial Laboratory, Center for Polymer Science and Technology, Department of Chemical Sciences, Tezpur University, Napaam-784028, Assam, India. E-mail: karakniranjana@gmail.com; Fax: +91-3712-267006; Tel: +91-3712-267009

<sup>b</sup>Biomaterial and Tissue Engineering Laboratory, Department of Biosciences and Bioengineering, Indian Institute of Technology Guwahati, Guwahati-781039, Assam, India

possess a sharp thermal transition ( $T_s$ ) near body temperature, as well as authors remain silent on the biodegradability and biocompatibility issues. It is pertinent to mention here that SMPs with  $T_s$  near body temperature is not only useful for the prevention of premature shape recovery but also helpful in minimization of cellular and tissue damages.<sup>14</sup> A transition temperature based on crystalline melting point ( $T_m$ ) of the soft segment of SMPs provides a fast and sharp transition.<sup>15</sup> Therefore, in this investigation, we focused on the development of a  $T_m$  dependent biocompatible, biodegradable starch modified HPU with desired shape memory behavior near body temperature, to complement the persistent global demand in the field of biomedical.

Henceforth, the present investigation highlights the development of a sustainable, biocompatible HPU using a starch modified hyperbranched polyol. So far, this has not been reported in relevant literatures. We have evaluated the mechanical and thermal properties of the product besides biodegradability and biocompatibility, and also its endurance as a thermo responsive SMP near body temperature to emphasize its potential as a safe and smart sustainable material for design of implant devices.

## Experimental

### Materials

Soluble starch with molecular weight 342.30 g/mol (Sigma-Aldrich, Germany), poly( $\epsilon$ -caprolactone) diol (PCL, Solvay Co.,  $M_n = 3000$  g/mol), polyethylene glycol (PEG, Merck, India,  $M_n = 600$  g/mol) and 1, 4-butanediol (BD, Merck, Germany) were vacuum dried overnight, prior to use. Bisphenol-A (BPA, Sisco Research Laboratories Pvt. Ltd, India) was used after recrystallization from toluene. Epichlorohydrin, (Sisco Research Laboratories Pvt. Ltd, India), sodium hydroxide (NaOH, Rankem, India), hydrochloric acid (HCl, 35%, Merck, India) and 2, 4/ 2, 6-toluene diisocyanate (TDI, Merck, Germany) were used as received. Tetrahydrofuran (THF, SD fine Chem., India) was used after distillation. Xylene (Merck, India) and dimethylacetamide (DMAc, Merck, India) were vacuum distilled and stored in 4A molecular sieves before use. All other chemicals used in this investigation were of reagent grade.

### Preparation of hyperbranched starch modified polyol (HBSP)

HBSP was prepared by a two-step method from soluble starch. The first step involved the condensation reaction where hyperbranched starch based epoxy (HBSE) was prepared by reacting starch with BPA and epichlorohydrin at 100 °C for 5 h, using NaOH as a catalyst.<sup>16</sup> The white, viscous epoxy resin was washed with brine solution followed by distilled water and vacuum dried at 70 °C. Similarly, HBSEs with 5, 10 and 20 wt% of starch with respect to BPA, were synthesized and coded as HBSE5, HBSE10 and HBSE20, respectively.

In the second step, HBSE was hydrolyzed with an amount of epoxy equivalent of dilute HCl for about 5 h at 70 °C. The hydrolyzed product was washed with distilled water for several

times to remove any trace of acid. This was confirmed by adding few drops of AgNO<sub>3</sub> solution in the washed off water, until there was no formation of white precipitate. The hydrolyzed product was dissolved in THF and dried under vacuum at 70 °C. Using the above technique HBSE5, HBSE10 and HBSE20 were hydrolyzed and coded as HBSP5, HBSP10 and HBSP20, respectively.

### Preparation of starch modified polyol based hyperbranched polyurethane (HPU)

HPU was prepared by the pre-polymerization technique in a three-necked round-bottomed flask equipped with a nitrogen inlet, a thermometer, a Teflon septum, and a mechanical stirrer. Required amount of PCL was taken in a reaction flask and dissolved in desired amount of xylene under constant stirring. DMAc solution of BD was added into it. At room temperature, desired amount of TDI was added drop wise into the reaction mixture, maintaining the NCO/OH at 0.9. The reaction was carried out at (70 ± 2) °C for 3 h in nitrogen atmosphere under constant mechanical agitation to obtain OH terminated pre polymer. In the second step, HBSP in xylene was introduced to the reaction mixture with the remaining amount of TDI at room temperature (overall NCO/OH = 1). The temperature was maintained at (80 ± 2) °C and stirred continuously for 4 h to complete the reaction as indicated by the absence of the isocyanate band at 2270 cm<sup>-1</sup> in the FTIR spectrum.<sup>6,13,17</sup> Using the same technique, three different HPUs viz. HPU5, HPU10 and HPU20 were synthesized using HBSP5, HBSP10 and HBSP20 as the branching moiety, respectively. Moreover, linear polyurethane (LPU) was also synthesized following the same technique, except PEG was added in the second step in place of HBSP. Small parts of the synthesized HPUs were precipitated in water, repeatedly for NMR analyses. The rest were cast on a glass slide and a galvanized tin sheet to obtain a film thickness of 1-2 mm for other tests and analyses.

### Instrumentation

Fourier transformed infrared (FT-IR) spectra were recorded on Nicolet (Madison, USA) FT-IR Impact 410 spectrometer in absorbance mode using KBr pellets. <sup>1</sup>H NMR and <sup>13</sup>C NMR spectra of the polymers were recorded by a 500 MHz AV500 AVANCE-III FT-NMR spectrometer (BROKER, Switzerland), using TMS as the internal standard and d<sub>6</sub>-DMSO as the solvent for <sup>1</sup>H NMR and <sup>13</sup>C NMR, respectively. UV spectra were recorded at room temperature (25 °C) using a Hitachi spectrophotometer (U2001, Tokyo, Japan). Thermal properties were evaluated by thermogravimetric analysis (TGA) and differential scanning calorimetric (DSC) studies. Thermogravimetric study was carried out by using a PerkinElmer 4000 thermal instrument, in the temperature range of (35-700) °C, at a scanning rate of 10 °C/min, maintaining an inert atmosphere of nitrogen at a gas flow rate of 30 mL/min. The differential scanning calorimetric study was done by a PerkinElmer DSC 6000, USA instrument in the temperature range (-50 to +200) °C (starting temperature = 0

°C) following a cycle of heating-cooling-heating under an atmosphere of nitrogen and at a scanning rate of 3 °C/min. Mechanical properties were measured by a Universal Testing Machine (UTM, Zwick Z010, Germany) equipped with a 500 N load cell operated at a crosshead speed of 50 mm/min for tensile strength (ASTM D 638) and elongation at break of samples with dimensions 10 × 1 × 0.02 cm<sup>3</sup>. The scratch hardness of the polymeric films was measured by a scratch hardness tester, Model No.705 (Sheen instrument limited, UK) with a stylus accessory at a travel speed of 30-40 mm/s. The specific gravity was determined by the standard procedure.<sup>6</sup> The intrinsic viscosity of the synthesized polymers was determined by Ubbelohde viscometer. The X-ray diffraction study was carried out at room temperature (25 °C) by a Rigaku X-ray diffractometer (Miniflex, UK) over a range of 2θ = (10-70)°. The surface morphology was studied by a scanning electron microscope (SEM, model JSM-6390LV (JEOL)), after platinum coating on the surface.

#### Shape memory study

The shape-memory behavior of the LPU and HPU films was studied using the following procedure. Briefly, the films were folded into a spiral shape at 60 °C (~T<sub>m</sub> + 20) °C for 5 min, which was immediately immersed into an ice-water salt bath at -(15 ± 5) °C for 10 min. The shape fixity of the cooled films was observed by drying them under vacuum and placing at room temperature for 30 min. Consequently, the fixed films were placed in a water bath at 40 °C, for which shape recovery and the time required to retain original shape was noted. A series of photographs were taken to show the shape-memory effect: (i) original shape (ii) temporary fixed shape (spiral) at room temperature, (iii)-(v) shapes in water bath at 40 °C after 5 s, 10 s, and 15 s, respectively, (vi) shape returning to its original form in water bath at 40 °C after 20 s, and (vii) shape in its original form at room temperature. The shape recovery and shape fixity were calculated from the following equations: Shape recovery (%) = [(90-θ)/90] × 100 ..... (1)

$$\text{Shape fixity (\%)} = [\theta/90] \times 100 \dots\dots\dots (2)$$

Where θ in degree, denotes the angle between the tangential line at the midpoint of the sample and the line connecting the midpoint and the end of the curved sample. The results are consistent as the test is repeated for five times.

#### Cell culture and proliferation assay

Primary human dermal fibroblast (HDF) cells were used to study cell proliferation activity on the polymeric membranes using alamar blue assay (Invitrogen, USA). HDF cells were cultured in high glucose Dulbecco's modified eagle medium (HDMEM, Gibco, USA) supplemented with 10% fetal bovine serum (FBS, Gibco, USA) antibiotics (Himedia, India), and 2 mM glutamine (Sigma- Aldrich, USA). HDF cells were cultured on the variants of polyurethane membranes such as LPU, HPU5, HPU10 and HPU20. Before culturing, the membranes (10 × 10 × 2) mm were sterilized using 70% v/v ethanol for 4 h and then washed with sterile phosphate-buffered saline (PBS, pH 7.4) to remove residual alcohol. Membranes were preconditioned

with HDMEM media for 24 h before seeding cells. Equal number of cells (2 × 10<sup>4</sup>) was seeded on each membrane as well as on tissue culture plate (TCP as control). Alamar assay was done on 1<sup>st</sup>, 3<sup>rd</sup>, 5<sup>th</sup> and 7<sup>th</sup> days following manufacture's protocol. Briefly, the cell-seeded membranes were incubated in medium with 10% (v/v) alamar blue dye for 3 h at 37 °C in a 5% CO<sub>2</sub> incubator following which 100 μL of solution from each sample was taken and read at 570/600 nm using a multiplate reader (Tecan infinite M 200). Non-seeded membranes were used as the negative control.

#### Live/Dead cell viability assay

Live/dead assay was done to check the viability and adherence of cells on the membranes after 7 days of culture. The cells were stained using staining solution containing 4 mM calcein AM (for live cells) and 2 mM ethidium homodimer (for dead cells) (Sigma-Aldrich, USA). Briefly, cell-seeded membranes were rinsed with PBS (pH 7.4) and incubated with live/dead solution for 15-20 min at 37 °C in humidified incubator. Excess dye was washed with PBS and cells were visualized under florescent microscope (EVOS FL, Life Technologies, USA). Viable cells convert calcein AM to calcein which imparts green color to the cells. However, ethidium homodimer enters into dead cells and fluoresces red after binding with DNA.

#### Nucleus staining method

Hoechst staining was done to stain cell nucleus on the membranes. The preconditioned sterile membranes were seeded with HDF cells (2 × 10<sup>4</sup>) and cultured for 7 days in complete HDMEM medium. On 7<sup>th</sup> day, membranes were washed three times with PBS (pH 7.4), followed by incubation in 3.7% formaldehyde in PBS for 10 min. The samples were further washed with PBS and preincubated with 1% BSA for 30 min. The constructs were then made permeable using 0.1% Triton X-100 for 5 min, followed by washing with PBS and staining with 5 μg/mL Hoechst 33342 for 30 min. Images were obtained using florescent microscope (EVOS FL, Life Technologies, USA).

#### Statistical analysis

All the above bio-related experimental data are reported as mean ± standard deviation (N = 4). Statistical analysis was performed by one way analysis of variance (ANOVA) using Microcal OriginPro 8 and differences between groups of *p* ≤ 0.01 were considered statistically significant.

#### Biodegradation study

Biodegradation study was done by McFarland turbidity method using *P. aeruginosa* as the bacterial strain.<sup>18,19</sup> A medium of mineral salts containing 2.0 g of (NH<sub>4</sub>)<sub>2</sub>SO<sub>4</sub>, 2.0 g of Na<sub>2</sub>HPO<sub>4</sub>, 4.75 g of KH<sub>2</sub>PO<sub>4</sub>, 1.2 g of MgSO<sub>4</sub>·7H<sub>2</sub>O, 0.5 mg of CaCl<sub>2</sub>·2H<sub>2</sub>O, 100 mg of MnSO<sub>4</sub>·5H<sub>2</sub>O, 70 mg of ZnSO<sub>4</sub>·7H<sub>2</sub>O, 10 mg of H<sub>3</sub>BO<sub>3</sub>·5H<sub>2</sub>O, 100 mg of CuSO<sub>4</sub>·7H<sub>2</sub>O, 1 mg of FeSO<sub>4</sub>·7H<sub>2</sub>O, and 10 mg of MoO<sub>3</sub>, all in 1.0 L of demineralized water, was prepared. It was sterilized for 15 min at 120 °C

under a pressure of 15 lb and then allowed to cool to room temperature. Bacterial strain of *P. aeruginosa* was cultured in the medium inside an incubator shaker at 37 °C for 48 h. 100 µL (108 microbes/mL, as calculated by McFarland turbidity method) of the cultured medium was taken in a conical flask containing 10 mL of the prepared salt medium. The LPU and HPU films were sterilized by autoclaving and were incubated inside the medium under sterile condition at 37 °C. The flasks containing mineral salt medium but without any bacterial strain was used as the control. The extent of biodegradation was studied from the measurement of weight loss (%) of the degraded LPU and HPU films, measured after 6 weeks of exposure to the bacterial strains, based on the following equation.

$$\text{Weight loss, } W = (W_0 - W_t) / W_t \times 100 \text{ ----- (3)}$$

Where  $W_0$  and  $W_t$  are the weights of sample before and after degradation, respectively, at the time of interest,  $t$ . The bacterial growth is indicated by increase in turbidity of the medium with time. The optical density (OD) of the microorganism was monitored by measuring the absorbance of the medium at 600 nm with respect to the control. The experiment was performed in triplicate. SEM images of the degraded films were taken to study their surface morphology after 6 weeks of bacterial degradation. The test was performed as per ASTM (American Society for Testing and Materials): D 5338-98 standard procedure.<sup>20</sup>

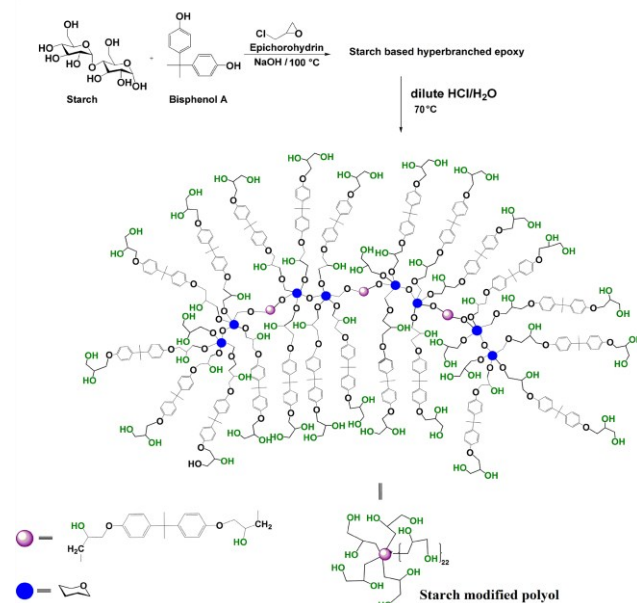
## Results and discussion

### Preparation and characterization of HBSP

In the present work starch was modified to a relatively more reactive HBSP, prepared by a two-step reaction approach. The proposed structure of HBSP20 is shown in Scheme 1. The first step entails the preparation of HBSE by condensation reaction of starch with *in situ* prepared diglycidyl ether epoxy of bisphenol A. While the second step involves the subsequent hydrolysis of HBSE by dilute HCl to prepare HBSP. The degree of branching (DB) and physical properties like hydroxyl value, solubility, viscosity etc. of the HBSP resins were obtained at three different wt.% of starch (HBSP5, HBSP10 and HBSP20) as given in Table 1. The hydroxyl value of HBSP is higher than HBSE due to ring opening reaction of the oxirane rings of HBSE on hydrolysis.

Table 1 Physical properties of HBSP

Property	HBSP5	HBSP10	HBSP20
Hydroxyl value (mg KOH/g)	328.08	386.56	429.31
Viscosity (dL/g)	0.427	0.376	0.316
Degree of branching (DB)	0.63	0.80	0.72



Scheme 1 Synthesis of HBSP20.

The hydroxyl value of HBSP20 was the highest due to the presence of the highest wt.% of starch (20%) in it, which resulted in a higher percentage of substituted branched epoxide units and subsequently higher number of hydroxyl groups, as compared to HBSP5 and HBSP10. The DB values of HBSE resins remained unaffected on hydrolysis as only the ring opening reaction of oxirane ring took place. Thus, HBSP resins had the same DB values as their respective HBSE resins on hydrolysis. The viscosity of HBSP20 was the lowest among the synthesized HBSP resins due to its highest DB that resulted in the formation of highly branched globular type structure bearing no entanglement. HBSP was found to be soluble in most of the organic solvents such as methanol, ethanol, acetone, THF, dimethylformamide (DMF), DMAc, dimethyl sulfoxide (DMSO), chloroform ( $\text{CHCl}_3$ ), dichloromethane ( $\text{CH}_2\text{Cl}_2$ ) etc. owing to the presence of a large number of functionalities along with the combination of aliphatic and aromatic moieties in the structures. This further supports the presence of hyperbranched structure in the synthesized polyol.

FTIR spectroscopy was used to confirm the variety of chemical functionalities present in HBSP5 as shown in Fig. 1 (i):  $\nu_{\text{max}}/\text{cm}^{-1}$  in FTIR  $1604 \text{ cm}^{-1}$  (ar C=C),  $3059 \text{ cm}^{-1}$  (ar C-H),  $1036 \text{ cm}^{-1}$  (alkyl ether),  $1247 \text{ cm}^{-1}$  (aryl ether) and  $3262 \text{ cm}^{-1}$  (O-H).<sup>16,18</sup> The FTIR spectrum of HBSP shows the disappearance of the sharp band near  $912 \text{ cm}^{-1}$  (asymmetric vibration of oxirane ring) unlike the spectrum of HBSE.<sup>16</sup> This confirms the ring opening reaction of the oxirane ring on hydrolysis of HBSE by dilute HCl. The  $^1\text{H}$  NMR spectrum confirmed the structure of HBSP as shown in Fig. 2 (i).  $^1\text{H}$  NMR ( $\delta\text{H}$  ppm, 500 MHz,  $d_6$ -DMSO (S),  $\text{Me}_4\text{Si}$ ): 3.8 (1H, CH of secondary hydroxyl group), 3.81 and 3.56 (2H,  $\text{CH}_2$  of primary hydroxyl group), 3.9 (2H,  $\text{CH}_2$  next to oxirane ring), 6.8 (4H, aromatic protons of bisphenol A), 7.1 (4H, aromatic protons of bisphenol A), 1.6 (3H,  $\text{CH}_3$  of bisphenol A), 3.7 (2H,  $\text{CH}_2$  next to bisphenol A).<sup>16,18</sup>

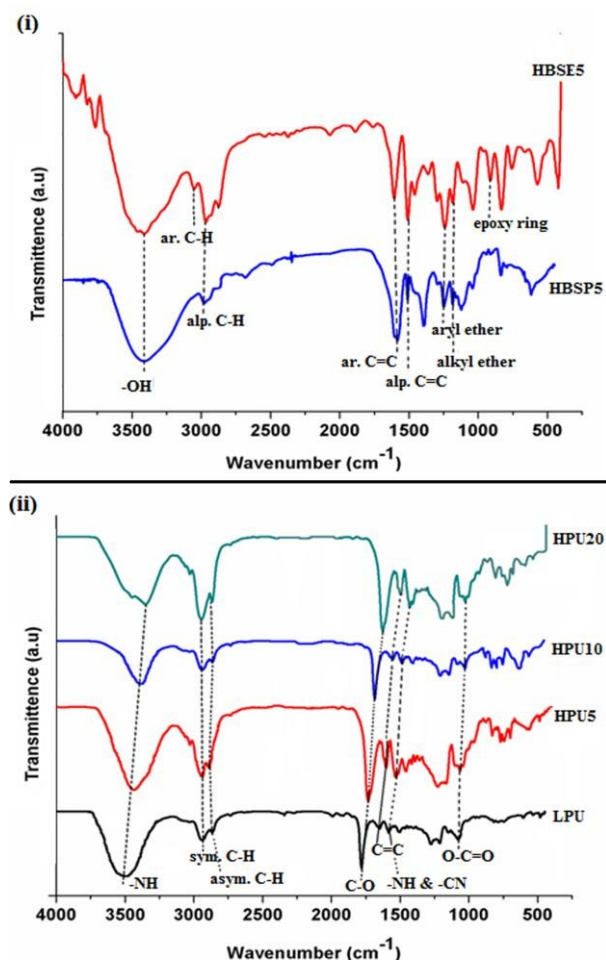


Fig. 1 (i) FT-IR spectra for HBSE5 and HBSP5 and (ii) HPU20, HPU10, HPU5 and LPU.

Signals at 4.1 (1H, proton attached with OH), 2.02 (1H, OH), 3.64 (1H, proton attached to C<sub>5</sub> of starch), 3.74 (1H, proton attached to C<sub>6</sub> of starch), 4.95 (1H, proton attached to C<sub>1</sub> of starch), 3.43 (1H, proton attached to C<sub>2</sub> of starch), 2 (1H, OH), 3.39 (1H, proton attached to C<sub>3</sub> of starch), 3.35 (1H, proton attached to C<sub>4</sub> of starch), 5.38 (1H, OH attached to C<sub>4</sub> of starch), 5.58 (1H, OH attached to C<sub>3</sub> of starch).<sup>16,18,21</sup> (C<sub>1</sub>, C<sub>2</sub>, C<sub>3</sub>, C<sub>4</sub>, C<sub>5</sub> and C<sub>6</sub> of starch are numbered according to the rules of IUPAC and designated as l, m, n, o, p and k, respectively in Fig. 2 (i)). In the same manner the carbons present in different chemical environments in the structure of HBSP20 were confirmed by <sup>13</sup>C NMR spectrum as shown in Fig. 2 (ii). <sup>13</sup>C NMR δC, ppm (d<sub>6</sub>-DMSO, S): 31.04 (CH<sub>3</sub>, bisphenol A), 66.7 (carbon of primary hydroxyl group), 71.7 (carbon of secondary hydroxyl group), 69.9 (carbon adjacent to secondary hydroxyl group), 114, 128.9, 143.2, 156.8 (carbons of bisphenol a moiety), 67-100.1 (carbons of starch moiety).<sup>16,21</sup>

### Synthesis of HPU

HPU was synthesized through a two-step, one-pot rearrangement reaction *via* A<sub>x</sub> + B<sub>y</sub> (x, y ≥ 2) technique using HBSP as the hyperbranched polyol moiety as shown in Scheme 2.

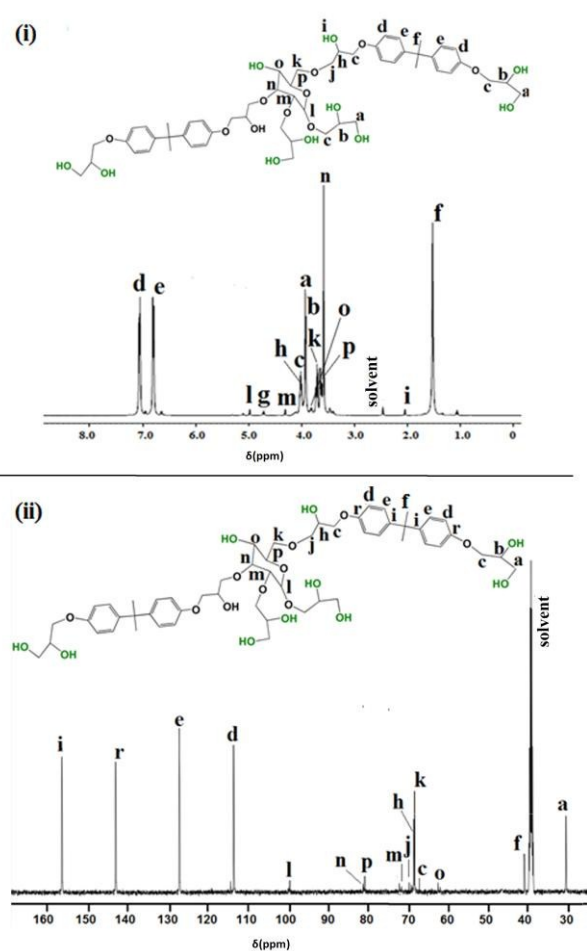
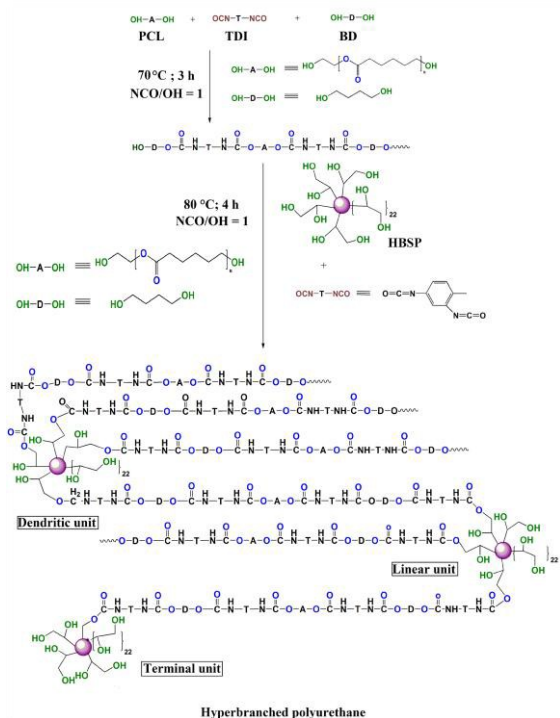


Fig. 2 (i) <sup>1</sup>H NMR spectrum of HBSP20 and (ii) <sup>13</sup>C NMR spectrum of HBSP20.

The first step involved the formation of -OH terminated pre-polymer (A<sub>2</sub> reactant) through the reaction of macroglycol (PCL) and chain extender (BD) with TDI at the required mol ratios (Table 2). The multifunctional moiety HBSP (B<sub>y</sub>) reactant was added in the second step and the reaction was performed carefully to obtain HPU without gel formation. The addition of HBSP at a relatively elevated temperature, use of the one-shot process and high concentration of HBSP (>15%) led to gel formation. Thus, in the 2<sup>nd</sup> step, a very dilute solution (15% in xylene) of HBSP was added at room temperature at slow rate. However, when the reaction was run at room temperature or a temperature lower than 80 °C, it did not produce the desired product. Thus, the reaction in the second stage was carried out by a stage wise increase of the temperature up to 80 °C to complete the reaction. The completion of the reaction was confirmed by the absence of -NCO band at 2270 cm<sup>-1</sup> in FTIR spectrum where the reaction mixture was directly taken from the reactor without any further purification. Further, the butyl amine test confirmed the completion of the reaction.<sup>22</sup>

### Characterization of HPU

The structures of HPUs and LPU were confirmed by FTIR in Fig. 1 (ii). The absence of absorption band for free -NCO at 2270 cm<sup>-1</sup> indicated the completion of the reaction.<sup>6,17,23</sup>



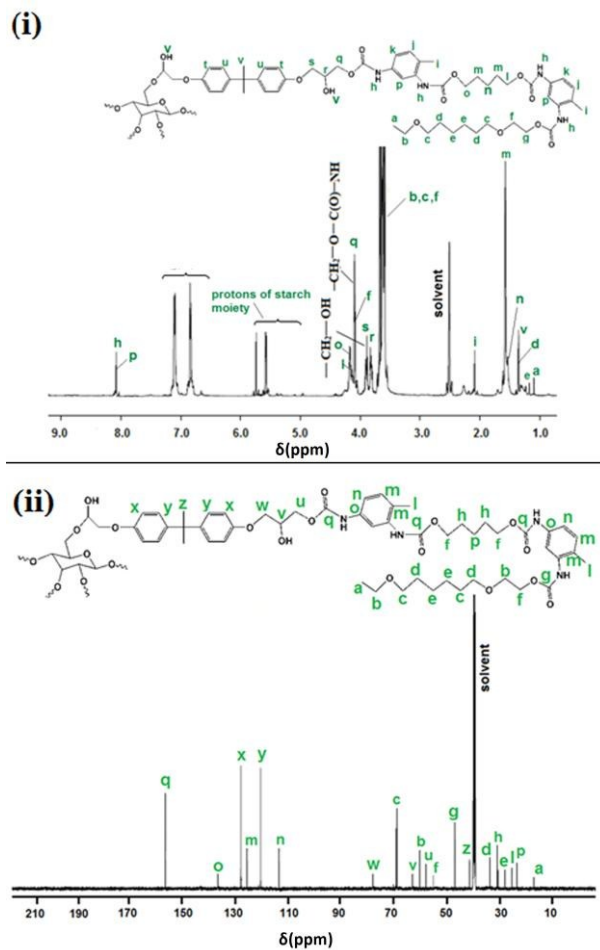
Scheme 2 Synthesis of HPU.

The absorption band near  $3200\text{--}3500\text{ cm}^{-1}$  can be attributed to the overlapping of O-H and N-H stretching vibrations. The intensity of O-H and N-H overlapping bands for HPU was higher than that of LPU owing to the presence of larger number of surface functionalities and hydrogen bonding. The bands near  $2945\text{--}2900\text{ cm}^{-1}$  (symmetric vibration of  $\text{CH}_2$ ),  $2830\text{--}2800\text{ cm}^{-1}$  (asymmetric vibration of  $\text{CH}_2$ ),  $1530\text{--}1550\text{ cm}^{-1}$  (C-N stretching/ N-H bending vibration),  $1040\text{--}1060\text{ cm}^{-1}$  ( $-\text{O}-\text{C}=\text{O}$  of urethane linkage) and  $1710\text{--}1730\text{ cm}^{-1}$  ( $-\text{C}=\text{O}$  of urethane linkage) were also found in the FTIR spectrum. The N-H/O-H stretching vibration was observed near  $3409\text{--}3438\text{ cm}^{-1}$ .<sup>6,13</sup> This is mainly due to H-bonding between N-H group and urethane carbonyl, PCL carbonyl or ether oxygen of PCL. A continuous shift of the N-H band from  $3438\text{ cm}^{-1}$  to a lower wave number  $3409\text{ cm}^{-1}$ , as a function of increase in the amount of TDI was observed in the FTIR spectrum.

Table 2 Composition (mol) of HPU and LPU

Reagent (mol)/Parameter	HPU5	HPU10	HPU20	LPU
PCL	0.002	0.002	0.002	0.002
Branching moiety, HBSP*	0.0029	0.0048	0.0068	0
PEG	0	0	0	0.0021
1,4-butanediol	0.004	0.004	0.004	0.004
TDI	0.0089	0.0108	0.0128	0.0081
Hard segment (%)	33	36	39	32
Soft segment (%)	67	64	61	68
HBSP (%)	11	14	17	0

\*HBSP5, HBSP10 and HBSP20 were used as branching moiety for HPU5, HPU10 and HPU20 respectively.

Fig. 3. (i)  $^1\text{H}$  NMR spectrum of HPU20 and (ii)  $^{13}\text{C}$  NMR spectrum of HPU20.

Similarly, in case of  $-\text{C}=\text{O}$  stretching frequency a gradual shifting from  $1710$  to  $1685\text{ cm}^{-1}$  was observed with increase in HBSP and starch content in HPU. This suggested that with increase in hard segment content the extent of H-bonding increases and demonstrated the different phase separation behavior among the polyurethanes.<sup>17,23</sup>

The structure of HPU20 was supported by  $^1\text{H}$  NMR spectroscopic analyses as shown in Fig. 3 (i).  $^1\text{H}$  and  $^{13}\text{C}$  NMR spectra of HPU20 indicated the presence of urethane linkage, HBSP, butane diol, PCL and TDI moieties. In  $^1\text{H}$  NMR  $\delta\text{H}$ , ppm (500 MHz,  $d_6$ -DMSO (S),  $\text{Me}_4\text{Si}$ ): the protons of allylic  $\text{CH}_2$ ,  $\text{CH}_2$  adjacent to oxygen atom of urethane group and  $\text{CH}_3$  of TDI showed peaks at  $\delta = 1.93$ ,  $\delta = 2.2$  and  $\delta = 2.45$ , respectively. Protons attached to  $\text{C}=\text{C}$  and aromatic protons appeared at  $\delta = 5.31$  and  $\delta = 7\text{--}7.6$ , respectively. Protons attached in aromatic group between two urethane linkages, adjacent to urethane linkage and adjacent to methyl group were found at  $\delta = 7.65$ ,  $\delta = 7.42$  and  $\delta = 6.99$ , respectively.<sup>17</sup> The DB of HPU was calculated by determining the intensity of the peaks of the substituted and unsubstituted hydroxyl groups from the  $^1\text{H}$  NMR spectrum of HPU (Table 2).

The  $^{13}\text{C}$  NMR also confirmed the structure of HPU20,  $\delta\text{C}$ , ppm (500 MHz,  $d_6$ -DMSO): the internal aliphatic carbon peaks

of the PCL segment appeared near 28. The smaller peak at 62.1 is associated with soft-segment carbons that are adjacent to a urethane linkage, while the peak at 53.9 is assigned to those soft-segment carbons that are adjacent to oxygen. The peaks near 28.4, 22.1 and 62.7 are attributed to methylene carbons of BD chain extender. The peak around 24 is attributed to methyl protons present in TDI. Three different peaks appeared for TDI carbons at 135, 117 and 129 for aromatic group between two urethane linkages, adjacent to urethane linkage and adjacent to methyl group, respectively.<sup>6,17</sup>

### Properties of HPU

Different physical properties of HPUs were evaluated. One of the most important characteristic of HPUs is the solubility. HPUs were found to be highly soluble in polar aprotic solvents such as DMF, DMAc, DMSO, THF etc. contrary to LPU, which was partially soluble in some solvents like DMAc, THF etc. This might be attributed to the compact globular structure of HPUs and presence of large numbers of polar surface groups.<sup>24</sup> The solution viscosity was slightly higher in LPU than in HPUs, owing to the hyperbranched structure of the latter as supported by the DB values (Table 3). The specific gravity of the polyurethane films varied from 1 to 1.06 with the increase of starch and HBSP content owing to the increase of compactness in the structure, as the number of polar groups increases with the same (Table 3). However, the values are within the normal range of the polyurethanes.

The surface morphologies of HPUs and LPU films were studied by SEM analysis in order to understand the distribution of soft and hard segments, which has strong influence on different properties. The SEM analysis revealed that the surfaces of HPUs and LPU were not smooth. There was a degree of non homogeneity, which may be attributed to the presence of soft and hard segments that leads to phase separation. The observed differences in the surface morphologies of HPU20 and LPU may be due to the difference in the extent of hydrogen bonding in their structures (Fig. 4). The presence of multi functional branching moiety in the hard segment of HPU20 enhanced the hydrogen bonding between hard segment-hard segment as well as hard segment-soft segment and hence the surface of HPU20 was rougher than LPU. The above two factors are responsible for the differences in the surface morphologies of HPUs and LPU.<sup>25</sup>

In order to study the arrangement of the molecular chains of LPU and HPUs, XRD analysis was performed. XRD study revealed two strong diffraction peaks near  $2\theta = 21.3^\circ$  and  $2\theta = 23.4^\circ$  due to the lattice plane corresponding to (100) and (200) of the PCL crystal as shown in Fig. 5 (i).<sup>26</sup> The position of the peaks remained same even after the incorporation of the branching moiety in the polyurethane structure, though the intensity gradually decreased with the increase of HBSP content. This is attributed to the increase in molecular restriction through intermolecular interactions with increase in HBSP content and decrease in the wt.% of crystalline PCL moieties in the matrix (Table 2).

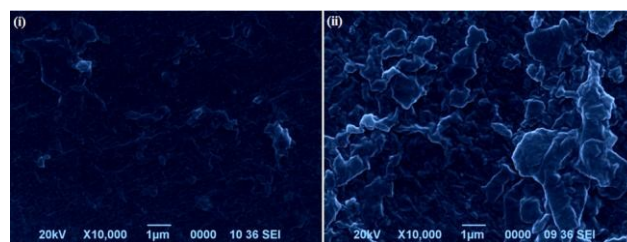


Fig. 4 SEM micrographs of (i) LPU and (ii) HPU20

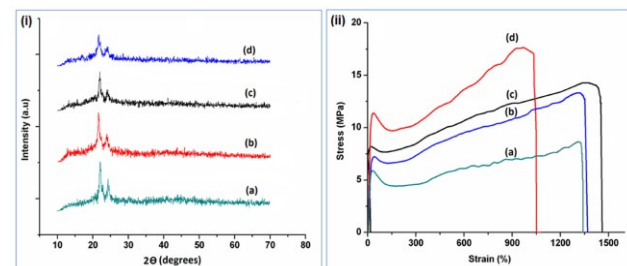


Fig. 5 (i) XRD patterns of (a) LPU (b) HPU5 (c) HPU10 and (d) HPU20, and (ii) Stress-strain profiles of (a) LPU (b) HPU5 (c) HPU10 and (d) HPU20

This resulted in comparatively less crystallinity in HPUs than LPU and the same was supported by DSC study.

Mechanical properties of HPUs and LPU were evaluated to examine their suitability as potential biomaterials. The results obtained for this purpose is tabulated in Table 3. Generally, mechanical properties depend on several factors *viz.* presence of hydrogen bonding, polar groups within the polymeric chains, existence of inter and intramolecular interactions, entanglement of chains, compositions and nature of reactants, molecular weight, rigidity of the polymer etc.<sup>17,27</sup> The tensile strength, scratch hardness and impact resistance increases whereas the elongation at break decreases with increase in starch content as well as wt.% of HBSP in HPUs. The addition of HBSP can favor the above factors by virtue of its rigidity and highly branched structure with polar functional groups as also supported by the DB values (Table 2).

Table 3 Mechanical and physical properties of HPU and LPU

Property	HPU5	HPU10	HPU20	LPU
Tensile strength (MPa)	13 ± 0.5	15 ± 0.5	17 ± 0.6	9 ± 0.5
Elongation at break (%)	1450 ± 10	1358 ± 8	1158 ± 10	1310 ± 7
Scratch hardness (kg)	5 ± 0.4	5 ± 0.3	6.5 ± 0.2	3.3 ± 0.2
Impact strength (cm) <sup>a</sup>	>100	>100	>100	>100
Toughness (MJ m <sup>-3</sup> ) <sup>b</sup>	146 ± 5	158 ± 3	163 ± 5	110 ± 6
Specific gravity	1.03	1.05	1.06	1
Degree of branching	0.56	0.65	0.79	-

<sup>a</sup>Limit of the instrument for impact strength was 100 cm (highest) and <sup>b</sup>Calculated by integrating the area under stress-strain curves.

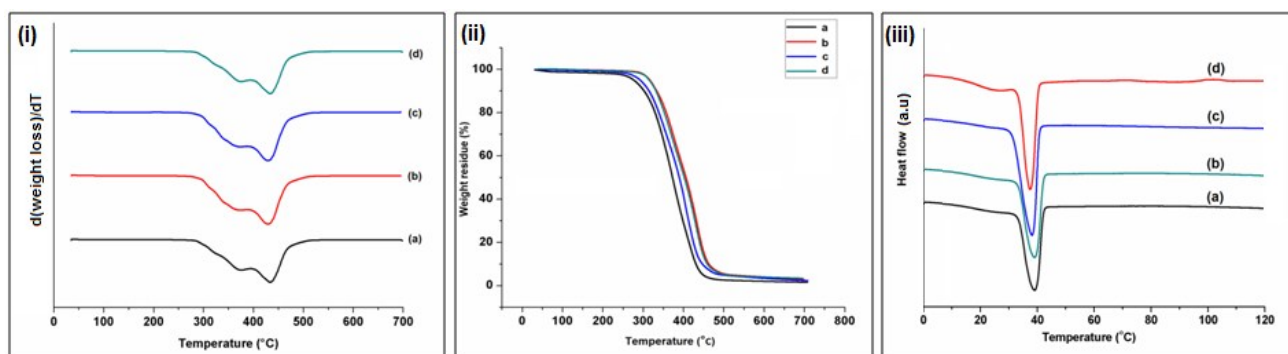


Fig. 6 (i) DTG curves of (a) LPU (b) HPU5 (c) HPU10 (d) HPU20, (ii) TGA thermograms of (a) LPU (b) HPU20 (c) HPU5 (d) HPU10, and (iii) DSC curves of (a) HPU20 (b) HPU10 (c) HPU5 (d) LPU.

HPUs exhibited the highest tensile strength and toughness (calculated from the stress-strain curve) while LPU the lowest as shown in Fig. 5 (ii). This is due to the predominance of the above factors in HPUs in comparison to LPU. HPU20 demonstrated the highest tensile strength and toughness as it contains the highest amount of hard segment as well as HBSP and starch content. This might be due to the increase in inter and intra molecular interactions, degree of hydrogen bonding and amount of aromatic moieties which increased with the hard segment and wt.% of starch and HBSP content.<sup>6,17,27</sup> Higher elongation at break was displayed by HPU5 and LPU in comparison to HPU10 and HPU20 as the latter exhibits higher DB and possessing compact globular structures. All HPUs and LPU films displayed excellent impact strength of 100 cm (upper limit of the used instrument), due to good polymer chain flexibility. The combined effect of aromatic and aliphatic moieties, different intermolecular interactions as well as the highest DB (Table 2) resulted in the three-dimensional network structure, contributing to the overall excellent performance of HPU20.

Moreover, the mechanical properties of the polyurethane films in the wet state were also determined by immersing the films in phosphate buffer solution (PBS) for 3 days, maintained at 37 °C in an incubator. The tensile strength, elongation at break and toughness of the films are found to be: LPU= 7.81 MPa, 1809% and 114.5 MJ m<sup>-3</sup>; HPU5= 13 MPa, 1423% and 151.7 MJ m<sup>-3</sup>; HPU10= 14.5 MPa, 1318% and 166.3 MJ m<sup>-3</sup>; HPU20= 16.6 MPa, 1919% and 298.2 MJ m<sup>-3</sup>, respectively. Thus, the mechanical properties of the films under the wet condition are not significantly affected, particularly for the HPUs and hence they can retain their mechanical property when implanted in the host body.

The thermal properties of polymers are also important for their various applications. The thermograms and derivatives of the thermograms of HPUs and LPU are shown in Fig. 6. The initial degradation temperature, peak temperatures for first and second stages of degradation and char residue at 700 °C are given in Table 4. In all the cases it was observed that the polyurethanes exhibited a two-step thermal degradation pattern (Fig. 6 (i)), as supported by literature.<sup>28</sup>

The initial degradation temperature ranging from 362-375 °C is attributed to the degradation of thermo labile aliphatic moieties and urethane bonds. HPUs exhibited a higher initial degradation temperature than that of LPU as the former possesses a compact hyperbranched structure with a greater number of secondary interactions than the latter. The peak temperature for second step of degradation ranges from 422-438 °C due to the degradation of aromatic rings belonging to TDI and HBSP moiety in HPUs and LPU. It is evident from the depicted thermograms that starch and HBSP content in the polyurethane can enhance the thermal stability of HPU, which is consistent with the wt.% of starch and HBSP in the polyurethanes (Table 4). The hyperbranched structure due to globular confined geometry owing to reactive multi-functional moiety HBSP, enhanced secondary interactions like hydrogen bonding, stronger intra and inter molecular structure contribute toward the better thermal properties of HPUs compared to LPU as shown in Fig. 6 (ii).<sup>21</sup> It is pertinent to mention here that an overlap of degradation steps was observed which may be due to the fact that during the degradation of aliphatic moieties, especially starch based ones, are transformed to thermostable aromatic moieties through decarboxylation followed by aromatization.<sup>16</sup> content due to the formation of carbonaceous products. This is indirectly supported by the observed higher thermal stability of HPUs as compared to LPU imparted by the aromatic moieties as well as enhanced secondary interactions like hydrogen bonding.<sup>27</sup>

Table 4 Thermal properties of HPU and LPU

Parameter	HPU5	HPU10	HPU20	LPU
Onset temperature (°C)	237	262	269	224
Peak temperature for 1st stage degradation (°C)	368	370	375	362
Peak temperature for 2 <sup>nd</sup> stage degradation (°C)	428	432	438	422
Weight residue (%)	2.4	2.9	3.4	1.4
Heat of crystallization (J/g)	75.18	73.39	70.32	77.36
Crystallinity (%)	55.27	53.89	51.70	56.88
Melting temperature (T <sub>m</sub> , °C)	38.03	39.12	40.2	37.9

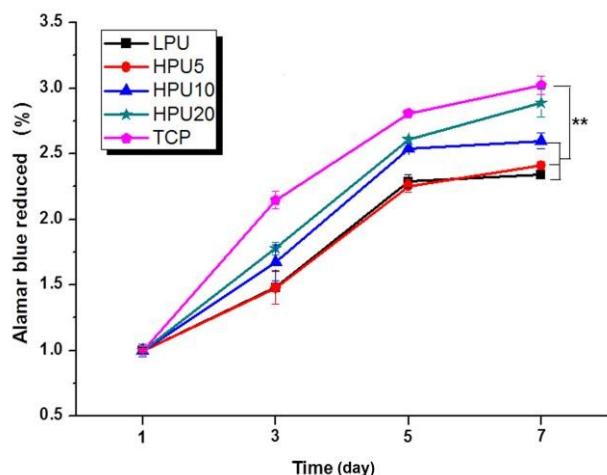


**Fig. 7** Alamar blue cell proliferation assay showing human dermal fibroblast (HDF) cell proliferation on HPU and LPU membranes. Data are plotted as means  $\pm$  standard deviation. (\*\*  $p < 0.01$ ,  $n=3$ ).

Further, weight residue left after degradation up to 700 °C also increased with HBSP and starch content due to the formation of carbonaceous products.

The melting transition temperature ( $T_m$ ) and heat of crystallization ( $H_c$ ) of HPUs and LPU were measured with the help of DSC as given in Table 4. The crystallinity of the soft segments of HPUs were determined by the measurement of  $H_c$  on cooling and with an enthalpy value of 136 J/g for 100% crystalline PCL. The  $T_m$  of HPUs increased with an increase in HBSP and starch content which leads to the formation of a compact structure through various types of interactions as stated earlier as shown in Fig. 6 (iii). This is due to the fact that starch exhibits a hydrophilic property which in turn leads to a large number of intramolecular interactions and strong intermolecular associations via hydrogen bonding formed by the hydroxyl groups in the structure.<sup>7</sup>

### Cell proliferation

Greater Alamar blue reduction directly relates to enhanced cellular metabolism and cell proliferation on the membranes.<sup>29</sup> The results show enhanced cell proliferation in HPU membranes containing starch as well as HBSP, as compared to LPU with no starch or HBSP content. In comparison to 1<sup>st</sup> day, cell proliferation on HPU20 films showed a 3-fold increment on 7<sup>th</sup> day. On other film variants the yield varied between 2.5-fold for HPU10 and 2.3 fold for HPU5 and LPU with  $p \leq 0.01$  (Fig. 7). The cellular growth was observed to increase with the HBSP and starch content in polyurethanes. On day 7, HPU20 (containing 20 wt.% of starch and 17 wt.% HBSP content) membranes showed the maximum cell growth with higher Alamar reduction reaching close to TCP control values followed by HPU10 (10 wt.% of starch and 14 wt.% of HBSP); HPU5 (5 wt.% of starch and 11 wt.% of HBSP) and LPU (without starch or HBSP content). There was significant difference between the TCP compared with LPU, HPU5 and HPU10 ( $p < 0.01$ ). However, no significant difference was observed between TCP and HPU20 ( $p > 0.01$ ).

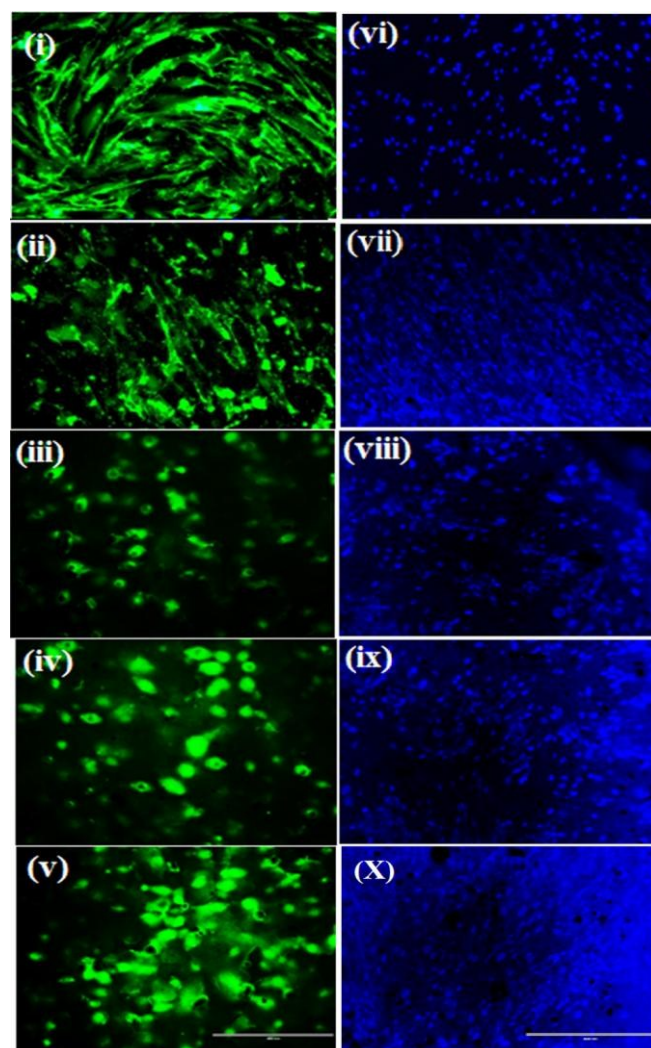


**Fig. 8** Fluorescent microscopic images of live/dead (i-v) and Hoechst (vi-x) staining showing human dermal fibroblast (HDF) cells growing on membranes after seven days of culture. (i, vi) tissue culture plate (TCP), (ii, vii) LPU (iii, viii) HPU5 (iv, ix) HPU10 and (v, x) HPU 20. \*Scale bar represents 400 mm

This effect may be due to the presence of higher amount of starch based polyol and starch content in HPU20. Starch supports cellular growth and is widely reported as biodegradable material for a range of biomedical applications including tissue engineering scaffold,<sup>30</sup> bone cements or drug delivery carriers.<sup>31</sup> The assay results indicate that the different membranes are cytocompatible for varied biological applications.

### Cell viability

Live/dead assay was performed to evaluate cellular viability and adhesion. As evident from fluorescent microscopic images, HDF cells were found to uniformly distribute and firmly adhere on the membranes. In comparison to control and LPU membranes where cells were found in their native spindle shape, HPU membranes exhibited rounded cell clusters (Fig. 8 (iii)-(v)) which may be an effect of starch and starch based polyol, present in the structure.

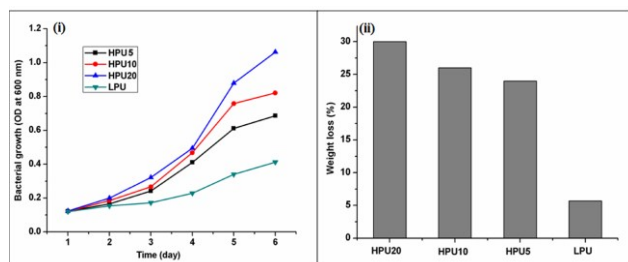


**Fig. 9** (i) Variations of *P. aeruginosa* bacterial growth against exposure time for polyurethanes, and (ii) Weight losses of polyurethane films after 60 days of exposure to the *P. aeruginosa* bacterial strain.

However, in all membranes no dead cell was observed after 7 days of culture suggesting material biocompatibility. Similarly, on staining with Hoechst dye prominent, rounded healthy nucleus were observed on all membranes, distributed throughout (Fig. 8 (vi)-(x)). This reaffirms that the material is highly biocompatible and can be used for various biomedical applications.

### Biodegradation

From the biodegradation study of HPU and LPU films, it was established that they were regularly degraded on exposure time by *P. aeruginosa* bacterial strain (Fig. 9). The differences in the cell wall structure of the gram negative bacteria, *P. aeruginosa* act as an active barrier which is supposed to control the degradation of the polymer substrate. It was found that the polyurethane films were degraded to a considerable amount after 6 weeks of inoculations by the used bacterial strain. This signifies that the polymer (carbon source) acted as catabolite to the bacteria.<sup>32</sup> The degradation was rapid for HPUs in comparison to that of LPU. Thus, HPUs were more susceptible to bacterial degradation. The well exposed and expanded hyperbranched structure of HPUs compared to LPU is more favorable for the attachment of the bacterial strain to form a bio-film which easily metabolized HPUs for extraction of nutrients. The growth of the bacterial strain was found to be the highest for HPU20, as it contains the highest amount of starch in its structure, and thus provides a better susceptible surface for bacterial growth, as evident from the OD curves (Fig. 9 (i)). The weight percentages of weight loss of the polyurethane films were found after 6 weeks of exposure to the bacterial strain which showed reduction in their weights. This is due to bleaching, dissolution, or degradation of starch by microorganism attack.<sup>33</sup> Also, as HPU20 consisted of the highest amount of starch in its structure, it exhibited the highest weight loss of 30% after 6 weeks of their exposure to the bacterial strain as shown in Fig. 9 (ii). The SEM images also revealed that HPU20 had undergone significant surface erosion and bacterial adherence as compared to LPU in the same time period by *P. aeruginosa* (Fig. 10). This may be due to the globular, confined structural geometry of HPU20 which is favorable for the easy penetration of the bacterial strain within the macromolecular structure of the polyurethane as their food source.

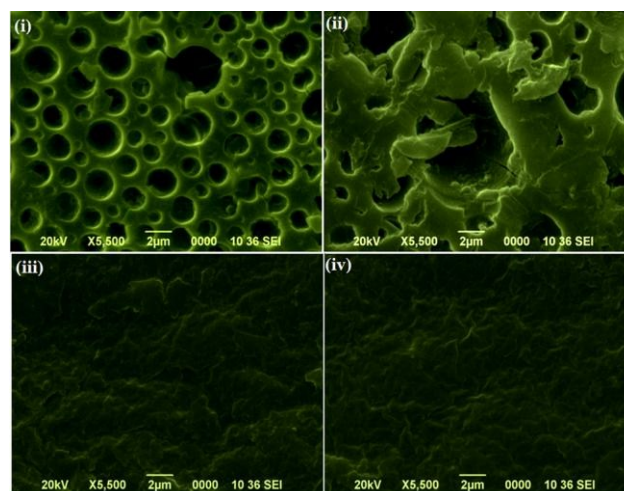


**Fig. 10** SEM images of (i) HPU20 and (ii) LPU after biodegradation; and (iii) HPU20 and (iv) LPU before biodegradation

The surface of the LPU film displayed only slight surface erosion (Fig. 10 (ii)) as compared to HPU20 due to the absence of starch content and presence of only biodegradable PCL moiety in the structure of LPU (Fig. 10 (iii)). Therefore, HPUs exhibited enhanced biodegradation compared to LPU. Thus from the biodegradation study it could be concluded that all HPUs are biodegradable and the rate of biodegradation is dependent on the starch and HBSP content.

### Shape-memory

The shape memory behaviors of the polyurethane films near body temperature are shown in Fig. 11.

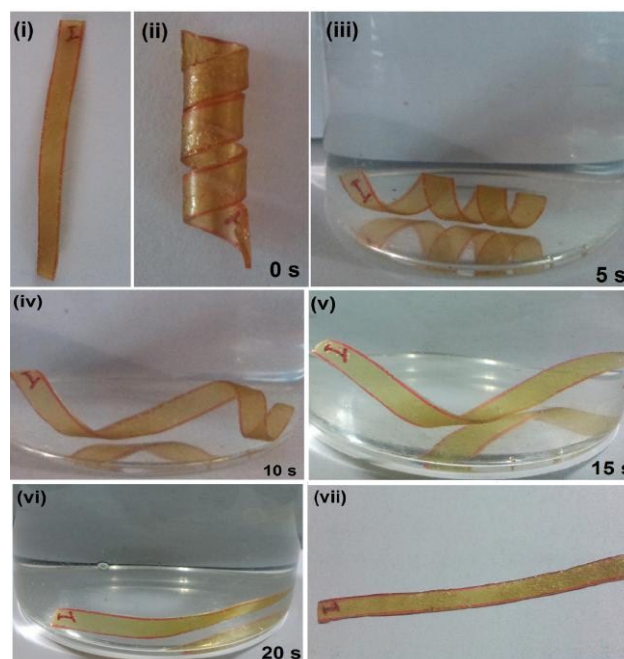


**Fig. 11** A series of photographs showing shape-memory effect of HPU20 film in water bath at 40 °C. (i) Original shape, (ii) Temporary fixed spiral shape at room temperature (iii) to (v) shapes in water bath at 40 °C after 5 s, 10 s, 15 s, respectively (vi) Shape returning to original form in water bath at 40 °C after 20 s, and (vii) Shape in its original form at room temperature.

Table 5 Shape memory properties of HPU and LPU

Property	HPU5	HPU10	HPU20	LPU
Shape recovery (%)	96.5±0.1	97.7±0.2	98.9±0.1	93.3±0.1
Shape fixity (%)	96.2±0.2	97.6±0.3	98.8±0.1	70±0.2
Shape recovery time (s)	21±1	21±1	20±1	25±1

The shape memory effect of SMPs is predominantly an entropic process. In the permanent shapes of the HPU and LPU films, the polymer chains are oriented in a random coil formation i.e., at their highest entropic state. When the HPU films are heated above their shape memory transition temperature at 60 °C ( $T_m + 20$ ), chain mobility is activated due to which they can be easily deformed into a temporary spiral shape, and their entropic state is lowered. The spirally folded HPU and LPU samples were then quenched into an ice salt bath for 5 min at  $-(15 \pm 5)$  °C, to fix the temporary spiral shape by kinetically freezing the polymer's molecular chains. Subsequently, when the mechanical stress was removed the polymer chains did not have sufficient energy to reverse the deformation. Upon reheating the films above their  $T_m$ , the molecular chain mobility is reactivated which allows the chains to gain entropy and return to the random coil motion.<sup>34</sup> The shape recovery of HPUs was increased with the increase in wt.% of HBSP (Table 5). Better shape recovery of HPUs compared to LPU is attributed to the increased stored energy of system due to uniform distribution of hard segments, multifunctional moiety HBSP and increased secondary interactions in the structure of HPUs.<sup>13,35,36</sup> HPUs also exhibited better shape fixity compared to LPU due to the hyperbranched structure of the former that enhanced the secondary interactions and the physical or virtual cross-links among the new orientated polymer segments upon cooling.

By deforming such heat sensitive SMPs above their  $T_m$ , a desired fit can be obtained and sustained after cooling. Therefore, such SMPs have potential biomedical applications in designing minimally invasive smart implants.

## CONCLUSION

The present study reported the synthesis of a biodegradable hyperbranched polyurethane using a starch modified hyperbranched polyol as a bio-based material with excellent yield, through a facile approach. The polymer exhibited remarkable mechanical performance at room temperature as well as under wet condition, high thermal stability, outstanding biocompatible attributes and exceptional shape recovery near body temperature. Furthermore, cell proliferation and live/dead cell viability assays confirmed the biocompatibility of the polymer. Thus, the starch modified polyol based tough biodegradable, biocompatible hyperbranched polyurethane has potential applications as an excellent physiological temperature responsive SMP in advanced biomedical applications.

## Acknowledgement

The author would like to thank Mr. Satyabrata Gogoi for helping in biodegradation study. Biman B. Mandal greatly acknowledges financial support by Government of India under the following grants DST- SB/FT/LS-213/2012 and DST-BT/PR6889/GBD/27/490/2012.

## Notes and references

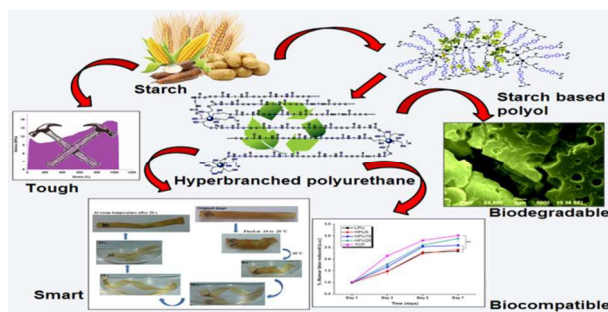
- H. Deka, N. Karak, R. D. Kalita and A. K. Buragohain, *Carbon*, 2010, **48**, 2013-2022.
- A. Lendlein, H. Y. Jiang, O. Junger and R. Langer, *Nature*, 2005, **434**, 879-882.
- S. Thakur and N. Karak, *New J. Chem.*, 2015, **39**, 2146-2154.
- A. Lendlein and R. Langer, *Science*, 2002, **296**, 1673-1676.
- X. Li, Z. Fang, X. Li, S. Tang, K. Zhang and K. Guo, *New J. Chem.*, 2014, **38**, 3874-3878.
- S. Thakur and N. Karak, *Prog. Org. Coat.*, 2013, **76**, 157-164.
- D. R. Lu, C. M. Xiao and S. J. Xu, *EXPRESS Polym. Lett.*, 2009, **3**, 366-375.
- H. Dave, P. V. C. Rao and J. D. Desai, *World J. Microbiol. Biotechnol.*, 1997, **13**, 655-658.
- Q. Wu, Z. Wu, H. Tian, Y. Zhang and S. Cai, *Ind. Eng. Chem. Res.* 2008, **47**, 9896-9902.
- A. L. Da Róz, A. A. S. Curvelo and A. Gandini, *Carbohydr. Polym.*, 2009, **77**, 526-529.
- Y. Lu and L. Tighzert, in *Novel plastics and foams from starch and polyurethanes. Biodegradable polymer blends and composites from renewable resources*, ed. L. Yu, Wiley, Hoboken NJ, 2008, 87-105.
- A. Saralegi, L. Rueda, B. Fernández-d'Arlas, I. Mondragon, A. Eceiza, M. A. Corcuera, *Polym. Int.*, 2013, **62**, 106-115.
- H. Kalita and N. Karak, *J. Appl. Polym. Sci.*, 2014, **131**, DOI:10.1002/app.39579.
- A. Lendlein and S. Kelch, *Angewandte Chemie-International Edition*, 2002, **41**, 2034-2057.
- L. Xue, S. Dai and Z. Li, *Biomaterials*, 2010, **31**, 8132-8140.
- R. Duarah and N. Karak, *RSC Adv.*, 2015, **5**, 64456-64465.
- B. Das, U. Konwar, M. Mandal and N. Karak, *Ind. Crop Prod.* 2013, **44**, 396-404
- B. De, K. Gupta, M. Mandal and N. Karak, *ACS Sustainable Chem. Eng.*, 2013, **2**, 445-453.
- M. Sponton, N. Casisa, P. Mazo, B. Raud, A. Simonetta, L. Rios, D. Estenoz, *J. Int. Biodeterior. Biodegrad.* 2013, **85**, 85-94.
- ASTM (American Society for Testing and Materials) Volume 08.03 Plastics (III) Designation: D 5338-98. *Determining Aerobic Biodegradation of Plastic Materials under Controlled Composting Conditions*, West Conshohocken, United States, 2004.
- T. Jordan, S. Schmidt, T. Liebert and T. Heinze, *Green Chem.*, 2014, **16**, 1967-1973.
- N. Karak, S. Rana, J.W. Cho, *J. Appl. Polym. Sci.*, 2009, **112**, 736-743.
- H. Deka and N. Karak, *Progress in Organic Coatings*, 2009, **66**, 192-198
- N. Karak, *Fundamentals of Polymers: Raw Materials to Applications*, PHI Learning Pvt. Ltd., New Delhi, 2009.
- C. Prisacariu, in *Polyurethane Elastomers. Morphology to Mechanical Aspects*, Springer Verlag, Wien, 2011.
- N. G. Sahoo, Y. C. Jung, H. J. Yoo, J. W. Cho, *Macromol. Chem. Phys.*, 2006, **207**, 1773-1780.
- S. Gogoi and N. Karak, *ACS Sustainable Chem. Eng.*, 2014, **2**, 2730-2738.
- I. Javni, Z. S. Petrovic, A. Guo, R. Fuller, *J. Appl. Polym. Sci.*, 2000, **77**, 1723-1734.

## ARTICLE

Journal Name

- 29 B. B. Mandal, A. Grinberg, S. E. Gil, B. Panilaitis and L. D. Kaplan, *Proc. Natl. Acad. Sci.* 2012, **109**, 7699-7704.
- 30 A. J. Salgado, P. O. Coutinho and L. R. Reis, in Novel starch-based scaffolds for bone tissue engineering: cytotoxicity, cell culture, and protein expression. *Tissue engineering*, 2004, **10**, 465-474.
- 31 C. S. Pereira, M. A. Cunha, L. R. Reis, B. Vazquez and S. J. Roman, *J. Mater. Sci.: Mater. Med.* 1998, **9**, 825-833.
- 32 T. Priya and G. Usharani, *Bot. Res. Int.*, 2009, **2**, 284-287.
- 33 H. S. El-Sheshtawy and M. M. Doheim, *Egypt. J. Pet.*, 2014, **23**, 1-6.
- 34 T. Lin, Z. Tang and B. Guo, *ACS Appl. Mater. Interfaces*, 2014, **6**, DOI:10.1021/am505937p.
- 35 Q. Meng, J. Hu, K. Ho, F. Ji, and S. Chen, *J. Polym. Environ.*, 2009, **17**, 212-224.
- 36 B. C. Chun, T. K. Cho, and Y. C. Chung, *J. Appl. Polym. Sci.*, 2007, **103**, 1435-1441.

## Table of Content



Starch modified polyol based tough biodegradable, biocompatible hyperbranched polyurethane with excellent thermoresponsive shape memory behavior near body temperature was demonstrated.